Annals of Science and Technology - A, Vol 5 (1): 45-55, 2020
Copyright: An Official *Journal* of the Nigerian Young Academy
ISSN: 2 544 6320

sciendo

ARTICLE

Application of Cellulose Acetate Reinforced Nanocomposite Fluorescence Film as Filter and Bio-Packaging Material with Antibacterial Properties

Yakubu Azeh,[1,3] * David O. Adetitun,[2] Gabriel A. Olatunji,[3]. and Folahan A. Adekola[3]

[1]Department of Chemistry, Ibrahim Badamasi Babangida University, Lapai, Niger State, Nigeria
[2]Department of Microbiology, Faculty of Life Sciences, University of Ilorin, Ilorin, Nigeria
[3]Department of Industrial Chemistry, Faculty of Physical Sciences, University of Ilorin, Nigeria

Received 22nd November, 2019, Accepted 27th March, 2020
DOI: 10.2478/ast-2020-0006

**Corresponding author*
D. O. Adetitun E-mail: adetitun.do@unilorin.edu.ng

Tel: +234-8036910988

Abstract

In an effort at developing new filters and bio-packaging materials with antibacterial properties, nanocomposite fluorescence films of cellulose acetate reinforced with cellulose nanoparticles, methylcellulose nanoparticles, propylcellulose nanoparticles, toluene diisocyanate modified cellulose and cellulose acetate nanoparticles were prepared and characterized. The effects of the nanoparticles on the mechanical, crystallinity and morphology of the nanocomposite films was studied. The sensitivity of bacteria against the new nanocomposite films was experimented. Scanning electron microscopy showed the films to be well dispersed. Modulus increase was directly proportional to nanoparticle loading. Samples with maximum compatibility were cellulose nanoparticles (CNPs) loading of 40% with modulus of 113.3Mpa and toluene diisocyanate modified cellulose nanoparticles (TDI-CNPs) at 20% loading had 146.0Mpa. Others include cellulose acetate nanoparticles (CANPs) at 30% loading with 73.0Mpa; methylcellulose acetate nanoparticles (MCNPs) with 5% loading had a modulus of 87.3Mpa and pure cellulose acetate had 45.0Mpa. The films were applied as filters for the removal of cells of *Bacillus; Enterococcus* and *Micrococcus* sp. from the crude bacteriocin, with recoverability of 95.9% based on the bacteriocin produced. The films showed limited antibacterial properties against clinical *Pseudomonas* sp 1, *Pseudomonas* sp 2 and *Proteus* sp. It is concluded that the films showed limited antibacterial properties hence it has antibacterial potentials and capabilities.

Keywords: Nanocomposite films, Filter, Fluorescence, antibacterial agents

BY-NC-ND *©2020 Azeh et al.* This work is licensed under the **Creative Commons Attribution-Non-Commercial-NoDerivs License 4.0**

1.0 Introduction

Continuity of antibiotic resistance is caused by the abuse of available drugs and lack of new drugs by the pharmaceutical companies. The reduction in new drugs is caused by reduced economic incentives and problematic regulations (Wright, 2014). The Centers for Disease Control and Prevention (CDC) had grouped some bacteria as present and continuing concern. This is due to the disease they cause in the hospital and the economic burden on the health care system, patients and their families and friends (Golkar et al., 2014).

The use of materials from petroleum-based products has raised serious environmental concern. This has led to increase in the use of natural polymers for continuous development and preservation of the ecosystem (Jinhui et al., 2013; Benyoussif et al., 2015). There have been spectacular developments and rapidly growing interests in renewable biopolymers obtained majorly from natural resources for a wide range of uses (Benyoussif et al., 2015). As nanoparticles, they have a unique strength and unique optical, electrical and magnetic properties. They are also capable of self-assembly. These versatile properties can be used to create a wide variety of new products including biocomposites or films, bio-plastics, iridescent coatings, wear-resistant surface treatments, and drug delivery systems. Natural fibres have been used in composites primarily as reinforcement phases. Many applications of natural fibres in the manufacture of composites for the automotive and other industries had been reported (Fogorasi and Barbu, 2017).

Nanocellulose filter papers with pore sizes between 2 and 200 nm have been used for the removal of viruses with sizes ranging from 12 to 300 nm (Giorgi et al., 2014). Organic membrane filters for virus removal have been developed by individuals and corporations. These filters are able to remove Human Immunodeficiency Virus (HIV), Hepatitis C Virus (HCV) with particle size in the range of 35-100 nm, and other viruses over a wide range of sizes (Zhao et al., 2008).

This study was set to prepare and characterize fluorescence nanocomposite films of cellulose acetate reinforced with CNPs, MCNPs, PCNPs, TDI-CNPs and CANPs and study the effect on the crystallinity, mechanical properties and morphology of the nanocomposite film. The nanocomposite films were prepared by solution casting-evaporation in acetone. The microstructure, mechanical properties, crystallinity and surface functionality of the nanoparticle reinforced cellulose acetate nanocomposite films were examined as a function of nanoparticle content by Fourier transform infrared spectroscopy, Scanning Electron Microscopy, Crystallinity and Mechanical tests. The structure and properties of the nanocomposite films were looked into to detect their possible application as antimicrobial filters, antibacterial agents and biodegradable packaging materials.

2.0 Experimental

Cellulose acetate, acetone and ethylene glycol, triethylamine and D-glucose were all purchased from BDH Chemicals Ltd (Poole, England). Polyether polyol, toluene diisocyanate were received as gifts from Vita foam, Lagos, Nigeria plc. All reagents were utilized as collected without any further treatment.

Preparation of nanocomposite films

Nanocomposite films were prepared using the synthesized nanocellulose and derivatives. The composite films were prepared using the solvent evaporation method described by Tanzina et al. (2012), with slight modifications. In brief, D-glucose (1.0 g) was dissolved in 2 mL of deionised water and stirred for 5 min., and then 1 mL of Ethylene glycol (EG) was introduced followed by the addition of 1 mL of polyether polyol and stirred for 10 mins. 30 mL of acetone was introduced into the D-glucose/EG/polyol mixture and stirred for 10 mins ensure homogeneity. Into this solution system was gradually added appropriate amount of cellulose acetate and stirred for about 30 min to complete dissolution followed by the addition of desired amount of the synthesized nanomaterials: 10, 20, 30, 40 and 50% respectively. The solution was stirred for 1 h until a viscous homogenous mixture was obtained at room temperature. Films were cast by pouring the film forming solution unto tiles/flat metal moulds and allowed to dry for 15 min at room temperature. Water was introduced to aid the peeling off of the solidified films. The peeled films were allowed to dry for 30 mins at room temperature. The films obtained were re-dissolved in 40 mL acetone at room temperature and stirred for 1 h and re-cast on tiles/metal mould. The films were treated with 1 % HCl solution and washed many times with distilled water to remove excess HCl present in the films. The films were further dried as described above for 6 h. The dried water insoluble films were stored in polyethylene bags prior to characterization and further analyses.

Synthesis of Anhydrous EDTA

Disodium EDTA (15.0 g) was solubilized in deionized water (200 mL), and concentrated HCl was added drop-by-drop until precipitation of the EDTA sets in. The white crystalline solid obtained was filtered, washed with ethanol 95 %, diethyl ether, and then dried in an oven for 15 mins at 105 ^{o}C and was left to cool in a desiccator (Andrea et al., 2013).

Preparation of nanocellulose-EDTA and Propylated nanocellulose-EDTA

The Cell-EDTA/ Propylated nanocellulose-EDTA was prepared according to the procedure described by Yoshifumi and Toyotoshi (2013) with a minor modification. Synthesized nanomaterials sample A2 (H_3PO_4-nanocellulose) and A11 (H_3PO_4-propylated cellulose nanoparticles-formed a clear solution which precipitated out upon addition of distilled water) were used as support materials. The chelating ligand, anhydrous EDTA was directly combined with the synthesized nanomaterials in a one-step synthetic procedure. In brief, 20 mL dimethyl sulfoxide was added to the mixture of (1.62 g (0.01 mol/10 mmol) Phosphonated-cellulose nanoparticles (A2) or 1.62 g (0.01 mol/10 mmol) Phosphonated propylcellulose nanoparticles (A11) and anhydrous EDTA 1.74 g (0.01 mol/10 mmol). The mixture

in a round bottom flask was stirred and heated for 2 h at 90 °C on a mechanical stirrer. Afterwards, the reaction mixture was filtered, and the nanoparticle immobilized with anhydrous EDTA was sufficiently washed with deionized water. The resulting product was then dried in air at 60 °C for 10 h and was kept for further analysis. The level of modification was measured by calculation in terms of weight percent gain (WPGs) based on weight differences of the treated samples before and after modification according to the equation below:

$$Weight\ percent = \frac{W2 - W1}{W1}\ x\ 100$$

Where $W1$ = initial weight before modification and $W2$ = final weight after modification

Modification using TDI

The modification of native cellulose and cellulose nanocrystals (A2, A11 and Native cellulose) was carried out by reacting 1.62 g (0.01 mol/10 mmol) of cellulose nanoparticle with 1.72 g (0.01 mol/10 mmol) of toluene diisocyanate (TDI) in 50 mL of toluene using triethylamine as catalyst for the diisocyanate reaction. The mixture in a round bottom flask was placed on a magnetic stirrer and was stirred at 90 °C for 24 h using Teflon coated magnetic bar. After this, the mixture was filtered and the yellowish residue obtained was washed with ethanol followed by deionized water and then air dried for seven days (Samuel and Wim, 2013). This was used for further analysis. Composite films were also prepared using the TDI- modified nanocellulose bearing the urethane linkage. The weight percent gain for the three samples (A2, A11 and native cellulose) was calculated using the formula above.

Screening of lactic acid bacteria for bacteriocin (bio-preservative) production

Lactic acid bacteria were propagated in 1000 mL of De Man Rogosa Sharpe (MRS) broth (pH = 5.8) at 30 °C for 48 h. for extraction of bacteriocins, a cell free solution of bacteriocin was obtained by centrifugation at 10,000 rpm for 20 mins. The culture was adjusted to pH 7 using 1 $moldm^{-3}$ NaOH to sequester the antimicrobial effects of organic acids. The supernatant obtained after centrifugation was filtered using two different cellulose acetate reinforced nanocomposite films prepared from the TDI-CNPs and the commercial 0.2 µm pore size cellulose acetate membrane filter to filter out the cells of bacteriocin producing organisms from the crude bacteriocin produced in order to compare the efficiency of the prepared nanocomposite films with that of the commercial cellulose acetate membrane filter. Inhibition activity from hydrogen peroxide (H_2O_2) was eliminated by the addition of 5 mg/mL catalase (Sani and Deme, 2013; Ekwem, 2014). In order to ensure the filtered broth was free of the producer cells, it was subjected to coloumetric analysis at a wavelength of 580 nm (Sani and Deme, 2013).

Collection of Bacterial Isolates

Bacterial isolates were collected from stock cultures at the Microbiology Laboratory, University of Ilorin Teaching Hospital (UITH) in Ilorin, Kwara State. The organisms were inoculated using already labeled inoculating loop aseptically into slant in sterile McCartney bottles. Each organism had duplicate slants giving a total of 10 slants.

Table 1: Bacteria used and point of isolation

Organisms	Point of Isolation
Escherichia coli	Intraperitoneal aspirate
Proteus sp	Wound swab
*Pseudomonas aeruginosa*1	Wound swab
Pseudomonas aeruginosa 2	Ear swab
Staphylococcus aureus	Wound swab

Preparation of Culture Media

Nutrient Agar, Nutrient Broth and Mueller-Hinton Agar were measured in to separate conical flasks as described by the manufacturers. The conical flasks were plugged with cotton wool and wrapped firmly with aluminum foil, then autoclaved at 121 ºC for 15 minutes.

Determination of Zone of Inhibition of Clinical Isolates

Disc test and Agar well diffusion methods were employed to test the antimicrobial susceptibility (Bauer et al., 1996).

Sterilization of Cellulose Acetate Reinforced Nanocomposite Films

The films were cut into disc shape using a perforator which was disinfected with 70 % ethanol and placed into labeled Petri dishes. The discs were sterilized using UV light for 1 h, turning the plate after the first 30 mins., to allow total penetration to ensure total elimination of any adhered microbes.

Bacteria Sensitivity Test using Cellulose Acetate Reinforced Nanocomposite Films

Mueller-Hinton agar was prepared in a conical flask and poured aseptically into sterile disposable plastic Petri dishes. The agar was left on the bench and allowed to set. Standardized concentration of inoculum, not longer than 24 h was inoculated onto the agar by streaking evenly across the plate using a sterile streak. The inoculum was allowed to dry for few minutes after which the acetate films were applied using a sterile forcep and pressed gently. The plates were incubated at 37 ºC for 18-24 h. The zone of inhibition (mm) was determined using a measuring ruler.

Preparation of 0.5 McFarland Standards

Approximately 85 mL of 1 % H_2SO_4 was measured into a 100 mL volumetric flask, a volumetric pipette was used to add 0.5 mL of 1.175 % anhydrous barium chloride ($BaCl_2$) drop wise to the 1 % H_2SO_4 while constantly swirling the flask. This brought the volume to 100 mL with 1 % H_2SO_4.

Standardization of Inoculum

The inoculum was standardized by comparing the turbidity of the test organism with 0.5 McFarland turbidity standards, which is equivalent to bacterial concentration of 1.5×10^8 colony forming units per mL (cfu/ml), which gives a confluent or semi confluent growth on the Mueller-Hinton agar after overnight incubation. The tube containing the inoculum was compared with tube of 0.5 McFarland standards by

viewing against a print car of sheet or white paper.

X-Ray Diffraction (XRD) Analysis of samples

X-ray diffractometry in reflection mode was carried out using a diffractometer system type, XPERT-PRO without monochromator. Anode material, Cu Kα1 and Kα2 radiation (λ1 = 1.540598 and λ2 = 1.544426 nm), with Kα ratio of 0.5 nm. Goniometer used was PW3050/60 (Theta/Theta); Minimum step size 2 Theta:0.001; Minimum step size Omega:0.001 with a fixed divergence slit and a receiving slit at 0.38 mm, generated at 45 kV and 40 mA at room temperature. Sample scan range of 5.021 - 90.00˚ 2θ in continuous scan mode with a step size of 0.02˚ at a rate of 101.49 sec was used. Four scans were used. The crystalline index of cellulose was calculated using Kim's empirical method:

$$CI = \frac{I002 - Iam}{I002}\ x\ 100$$

Where CI is the crystallinity index, I_{002} is the maximum intensity and represents crystalline material, while Iam represents maximum intensity of the amorphous material.

FT-IR results of Cellulose, Methylcellulose and Cellulose acetate nanoparticles

The FT-IR spectra of samples were recorded FT-IR-8400S Fourier Transform Infrared Spectrophotometer in the spectra range of 4000-400 cm^{-1}. Samples were run as KBr pellets.

Scanning Electron Microscopy

The surface morphology of the samples was carried out using JEOL scanning electron microscope with magnification value of 1000. SEI signal with EMI -Current 9.00, SM-Probe-Current 0.00 and SM-Penning-Vac 9.634e-005.

Measurement of mechanical properties

Film thickness

Thickness of the films (25–35 mm) was measured using a Mitutoyo digimatic Indicator (Type ID-110E; Mitutoyo Manufacturing Co. Ltd, Tokyo, Japan) with a resolution of 1 m, at five random positions around the film, by slowly reducing the micrometer gap until the first indication of contact.

Tensile strength, tensile modulus and elongation at break

Tensile strength, tensile modulus, elongation at break, tensile energy of absorption (TEA), force at break, Tensile energy absorption index, force at peak, tensile index and tension length were tested using a Universal Tensile Machine (Model Fisher Scientific (FS)300CT, England) equipped with a 100 N-load cell (type FBB) and 1.5 kN-specimen grips. The dimensions of the rectangular shape test specimen were test Speed, 10.000 mm/min, Width: 60 mm, Sample Length: 100 mm and Film Weight: 6 g/m^2.

3.0 Results and Discussion

Weight percent gains due to modification using EDTA

The weight percent gain is indicated in table 2 and table 3.

FT-IR Spectra of composite films

FT-IR analysis was carried out to characterize the incorporation of CNPs, CANPs, MCNPs and propylated cellulose nanoparticles (PCNPs) into the cellulose acetate-based composite films and monitor the changes in FT-IR absorption bands and vibration shifts related to the interaction of cellulose nanoparticles and its derivatives. The nanocomposite films **Figure 1**, Showed dominant peaks from 3503-3393, 2980-2870, 1749 and 1363 cm^{-1} respectively. The broad absorption band at 3503 – 3393 cm^{-1} has been assigned to ─OH stretching vibrations of cellulose nanoparticles (Simone et al., 2012; Saxena, 2013; Meiling et al., 2013). This band seems broadened with increased nanoparticle contents for some of the synthesized nanomaterials used as reinforcements. This trend indicates an increase in hydrogen bonding network between the nanoparticles and cellulose acetate matrix. The broadening of this peak may be due to strong hydrogen bonding network of the nanoparticles. The peak appeared to have reduced in all pure synthesized nanoparticles. The band at 2870 cm^{-1} corresponds to C-H stretching vibration of -CH_2 (methylene) and symmetry vibration of the aliphatic CH_2 group in acetate (Saxena, 2013; Meiling et al., 2013; Nor et al., 2014). This peak appeared in all composite films and was observed to have shifted to higher frequency in the films compared to the absorption of this band in pure nanoparticles at 2725-2724 cm^{-1}, peak position. A shoulder appeared in pure cellulose acetate nanoparticles around 2969-2953 cm^{-1}. This shoulder appeared at higher absorption band around 2980 cm^{-1} in all composite film samples with various degrees of intensities which depend on the amount and type of the nanoparticles used as re-inforcement. This band was characteristics of the propyl ($CH_3CH_2CH_2$─), methyl (CH_3─) and acetyl (CH_3CO─) groups.

This was evidence that the nanoparticles as re-inforcement were well dispersed into the matrix of the bulk material. The presence of the band absorption observed at 2895 cm^{-1} has been associated with poly ether polyol and ethylene glycol -CH_2 units in the matrix of the nanocomposite films. This peak intensity increased when the nanoparticle content was 30 %. In pure MCNPs nanoparticles synthesized. This peak was intense but with flat bottom. However, with the addition of MCNPs, the peak decreased to lower frequency. This observation was an indication that the surface of the film was cemented by the MCNPs. A similar observation was reported (Monique et al., 2011). The peak at 1363 cm^{-1} bending vibration was an indication of the presence of the repeat units; –CH_2-CH_2-CH_2O- and CH_2-CH_2-O- of the polyether polyol (PEPOL) and EG cross-linkers. The intensity of this peak in films was approximately similar, probably due to the fixed amount of PEPOL/EG in film compositions. The intense peak observed at 1749 cm^{-1} which appeared in all composite films corresponds to stretching vibrations of carbonyl (C=O) assignable to acetyl group in the composite composition (Saxena, 2013; Yoshifumi and Toyotoshi, 2013). As expected, this absorption band shifts to higher bands in composite films (1749 cm^{-1}) compared to pure nanoparticles (1716 cm^{-1}), due to retention and/or mixing of the filler material in the matrix. The intensity of this peak decreased with increased in NPs contents in the films and this agreed with the report by Monique et al. (2011); Andrea et al., (2013). Thus, the hydrophilicity of the films had decreased due to addition of cellulose acetate. The

 This journal is © The Nigerian Young Academy 2020

band at 1680 cm^{-1} is due to free carbonyl carbon of the glucose unit and appeared at higher absorption band in films. The band corresponding to asymmetric bending vibration of $–CH_3$ due to acetate was observed at 1480 cm^{-1}. The shift in this band to higher frequency was attributable to methyl groups in cellulose acetate and the propyl and methyl groups in propylated and methylated nanoparticles. It was observed that composite films prepared from PCNPs and MCNPs were glossy and thus, had poor water retention ability.

The band at 1410 cm^{-1} has been attributed to C-O stretching vibration which was similar in all nanocomposite films. The characteristic cellulose backbone ranged from 1051 – 610 cm^{-1} (Kalia, 2011; Renata et al., 2012; Saxena, 2013; Simone et al., 2012; Meiling et al., 2013). These peaks correspond to C-O-C, C-OH, C-C and C-H which are responsible for the following vibrations: 1051 cm^{-1}, due to pyranose ring skeletal stretch, while the small broad band at 904 cm^{-1} is unique to β-linkage between sugar units. This band is sharp in pure nanoparticles. This peak was due to the presence of crystalline organization of nanoparticles and strong hydrogen bonding of the nanoparticles with accessible -OH groups and –C-O-C (glycosidic linkage) in cellulose acetate. It was observed that the peak became broadened with increasing nanoparticle contents for Sample A2(0.3) and A2(1.0). This also caused the disappearance of the band at 890—800 cm^{-1}, which corresponds to C-H rocking vibrations in cellulose II, attributable to cellulose acetate in films. The sharp peak with high intensity at 1050 cm^{-1} in the films appeared to be due to a shift in the band position at 1184 – 1060 cm^{-1} due to C-O stretch of the glucose units. It was observed that this band collapsed resulting in its disappearance in the films. Also observed were the disappearance of the bands at 1032, 1030, 1003 and 997 cm^{-1} and the appearance of the band at 900 cm^{-1} (cellulose II) in composite film due to the presence of amorphous cellulose acetate, MCNPs and PCNPs (Yiying, 2007). This suggests some chemical interactions occurred between the components in the nanocomposite films.

FT-IR Spectra of EDTA and TDI modified cellulose nanocrystals

The success of modification was confirmed with FT-IR spectra data **Figure 2**. The broad band observed around 3340 - 3280 cm^{-1} is attributed to N-H symmetric stretch (Pacheco et al., 2012). Absorption due to CH for the CH_2 group in CNC-EDTA modified sample was observed around 3020 cm^{-1}. This shift to high absorption is due to N-C bond. The carbonyl stretching vibration due to COOH in EDTA modified sample appeared around 1680 cm^{-1} while that for the TDI modified sample appeared at 1650 cm^{-1}. The absorption bands characteristics of cellulose structure appeared in both modified samples around 1110 - 450 cm^{-1}. Aromatic stretching vibration was evidenced by the presence of absorption band at 1520 cm^{-1} for C=C of the phenyl group in TDI modified sample. The absorption band at 1590 cm^{-1} due to N-H stretching vibration also confirmed the formation of urethane bond (cellulose carbamate). The band at 1410 -1000 cm^{-1} is due to C-O vibration (Youssef et al., 2006). The N-H symmetric stretching was seen around 1320 cm^{-1} for the EDTA modified sample. The peak at 1220 cm^{-1} and 1650 cm^{-1} are ascribed to C-N and C=O stretching vibrations and their presence are indication of the formation of urethane bond confirming the formation of cellulose carbamate and the success of modification.

Morphological study of nanocomposite films using scanning electron microscopy (SEM)

The morphology of the fractured (cross-section), Plate 1 of the prepared nanocomposite films was studied using SEM in order to confirm structural changes that may occur due to nanoparticle contents and/or differences in the structural arrangement due to composition of the reinforcing material and the bulk matrix interactions. Cross-section images at different magnifications showed appreciable surface compatibility and uniform dispersion of nanoparticles in the matrix of the bulk material (Perera et al., 2014; Samzadeh et al., 2016). The composite films also showed good evidence of strong interactions between the reinforcement and the matrix materials as shown by their smoothness, cellular web, lamellar and stacking morphological and a tridimensional network (Fernando et al., 2012). Intermolecular cohesion was observed in the composite films as shown by the cross-section of SEM micrographs. In addition, the formation of hydrogen bonding between the filler materials and the matrix coupled with interactions with plasticizers used, enhanced the observed even distribution of the filler into the cellulose acetate matrix (Andrea et al., 2013). The smoothness of the inner surface of the composite films was obviously due to complete surface miscibility of the component materials in the composite. The composite films, though of different nanoparticle composition displayed similarities in their structure, as it is evidenced by the presence of large and small pores that are evenly distributed across the film structure. It was observed also that the nanoparticle distribution in the matrix material appeared as white round particles bound by cellulose acetate matrix in agreement with literature (Lexa, 2014). Smoothness was also attributed to effective stirring during processing. These features have been found essentially good for reverse osmosis (RO) membrane/film performance (Perera et al., 2014). The effect of cellulose nanoparticles (CNPs) as fillers was observed for the filler content at 30 and 40 wt % as shown by the presence of large porous cellular structure. This was not seen in the composite films loaded with CNPs content at 10, 20 and N2(20) wt % (EDTA treated film) as these films showed smaller porous network with N2(20) (EDTA-treated film) displaying more number of smaller porous network structure, which was attributed to possible occupation of the porous (cavities) network by the absorption of EDTA and water molecules (Perera et al., 2014).

Composite films formulated using cellulose acetate as bulk material and reinforced using MCNPs and PCNPs nanoparticles were characterized by uniform distribution of both large and small pores. The reason for this was attributed to the presence of methyl and propyl groups in their structures, brought by the occupation of large volume of space in the films. The uniformity in the cavities observed in the composite films was also due to non-variations in the quantity of the additives, ethylene glycol (EG) and polyether polyol. The formation of voids in the film structure was responsible for the decrease in the mechanical properties observed on the prepared films as indicated by their tensile strength and modulus, since the material is more likely to break in those regions. This also agreed with (Kusworo et al., 2014) finding on porous cellulose acetate membrane prepared for water

softening. Generally, the nanocomposite films have a dense skin layer at the bottom over-laid by small and large cavities covered by a thin skin surface layer at the top similar to other reports (Wienk et al., 1996; Kusworo et al., 2014). The above description of the film structure is similar to that of asymmetric cellulose acetate membrane structure (Kusworo et al., 2014).

The porosity of the prepared nanocomposite films has been linked especially to glucose and polyether polyol as plasticizers/additives in the composition due to their large molecular mass, since the addition of a macromolecular additive increase the surface porosity of a material (Wienk et al., 1996). In addition, the enhancement of pores in the film has been linked to polyether polyol (PEP) and EG due to their viscosity. The modification of pores in polymer composite has been linked to addition of viscous oil/plasticizers (Fernando et al., 2012). Thus, the porosity of the prepared nanocomposite films can be controlled by varying the amount of EG and polyether polyol in the formulation. The polyether polyol also serves as a cross-linker between the cellulose acetate matrix and nanoparticles via their free surface -OH groups which is also able to form bonds through self-assembly with another polyether polyol molecule via the terminal -OH groups, creating flexible links on its structure. This process probably gave rise to the formation of open-cell network and flexibility of the nanocomposite films (Wienk et al., 1996). The porous structure may be due to film processing conditions such as inability to degas the film forming solution to remove any trapped gases during processing. The porosity of the films is however essential for the absorption of gases, sound insulation and use as molecular sieves. This implies that the films may find application in electronics as acoustic diaphragms. The pores are also of importance in controlling the water moisture absorption and release rate in medical applications as wound dressing materials (Fernando et al., 2012). The composite films showed blue fluorescence when viewed under the UV-lamp at long wavelength **(Plate 2)**. This property of the films could find useful applications as good and fast analytical tools as fluorescence chemo-sensors/biosensors.

XRD of the studied nanocomposite films with different compositions

Diffractograms of composite films had peaks related to the crystallographic planes of cellulose in accordance with the Bragg angles at 2 Theta **Figure 3**. The observed peaks have been identified as the crystalline cellulose nanoparticles (CNPs) diffraction peaks 15.5^o (110), 18.9^o (101), 22.5^o (002), and 43.8^o (040) in composite films are all characteristic peak of cellulose I crystals (Samzadeh et al., 2016). The characteristic CNPs peak at 22.5^o is broad and appeared in all samples containing CNPs particles with the exception of MCNPs and PCNPs composite films. This further confirmed the even distribution and miscibility of nanoparticles in the cellulose acetate matrix as revealed by SEM studies of the nanocomposite films. The absence of the characteristic CNPs peak in MCNPs and PCNPs loaded composite films indicates the absence of CNPs in their composition due to transformation of the cellulose I to cellulose II during methylation and propylation of native cellulose. Hence, these two composite samples exhibited only the characteristic peak for cellulose II at 2θ = 18.1^o as expected. The broad pattern observed was due to dispersion of nanoparticles into the cellulose acetate matrix, resulting in decreased crystallinity as reported (Syuhada et al., 2014). It was observed that the intensity of the peak differs with respect to nanoparticle contents in the prepared nanocomposite films. The peak intensity increased in the following order; 40 > 30 > N2(20), which was due to cellulose I nanoparticle content in the sample. The presence of the observed peak intensities in the sample was an indication of the CNPs content in the film matrix (Huang et al., 2011; Yucheng et al., 2013). The observed peak at 29.4^o was due to increased crystallinity attributed to CNPs content in the films. The crystallinity index of the composite films was 16 % compared to 25 – 80 % of pure nanoparticles and its derivatives synthesized. This decrease in crystalline index was attributed to the dispersion of CNPs into the amorphous cellulose acetate matrix as shown by SEM images. The peak observed at 7.8^o for the MC nanoparticle loaded composite films was attributed to cellulose crystallinity due to modification and /or glucose type crystalline order in native MC (Nadezhda et al., 2011). A shift of this peak from 7.8^o to 9.2^o is due to degradation of the amorphous cellulose during acid hydrolysis. The crystallinity index for the EDTA and TDI modified samples **(Figure 4)** was 20.3 % as a result of the CNPs in composite films. An increase in crystallinity was observed for the EDTA modified sample at 29.7^o. Peaks due to CNPs were observed at 2θ ranging from 22.7 - 27.2^o for the (002) crystallographic plane **Figure 4**. The peak at 18.1^o is assigned to the presence of amorphous portion/cellulose II crystallographic plane (101) (Yucheng et al., 2013). The observance of this peak was attributed to the presence of cellulose acetate matrix. Treatment with EDTA increased the crystallinity of the sample due to the formation of a stable complex with cellulose nanoparticles as indicated by its sharp peaks. TDI modified sample showed two major broad peaks only at 2θ =15.8^o and 22.7^o (Marianne et al., 2007; Yucheng et al., 2013) for the cellulose I and II crystalline planes (101) and (002) respectively. The shift in the peak at 18^o in TDI modified sample could be attributed to the formation of new linkage during modification.

Mechanical properties of the studied nanocomposite films

The mechanical features such as, tensile, modulus, elongation at break, tensile energy of absorption (TEA), force at break, Tensile energy absorption index, force at peak, tensile index and tension length of the prepared nanocomposite films were evaluated. It was observed that nanoparticles increased the modulus of the films as shown by the values of young`s modulus. The increase in modulus varied due to nanoparticle content in the samples and was linked to more number of interfacial interactions between individual nanoparticle and the bulk matrix (Marielle et al., 2007). For the CNPs, 40 wt % nanoparticles loading had a modulus of 113.290 Mpa while 10 wt % loading had 52.585 Mpa. The TDI modified sample had 145.965 Mpa at 20 wt % nanoparticle loading. Increased loading to 30 wt% of the TDI-CNC nanoparticles led to a drastic fall in the modulus of the film to 41.063 Mpa. The cellulose CANPs at 30 wt % loading exhibited 73.035 Mpa while the MCNPs suspension with 5% loading had a modulus of 87.252 Mpa. The controlled cellulose acetate film and the commercial cellulose acetate membrane film had a modulus each of 42.827 and 65.472 Mpa respectively. These values confirmed the effect of

 This journal is © The Nigerian Young Academy 2020

nanoparticle loading in the nanocomposite films. (Wan et al., 2009) reported an increase in modulus and tensile strength for starch/BC reinforced composites with BC loading ranging from 7.8 to 22 wt %. However, elongation at break of composite films decreased with increasing nanoparticle loading. The nanocomposite films had high mechanical properties than the pure cellulose acetate films, which was attributable to the reinforcing effects of nanoparticles. The modulus of the films was linked to the formation of hydrogen bonding, filler size, surface compatibility and dispersibility of the filler in the bulk cellulose acetate matrix (Syuhada et al., 2014).

The high values of young`s modulus obtained with the TDI modified sample could best be explained by the interactions of the hydrophobic phenyl groups of the isocyanates with the hydrophobic acetyls of the bulk cellulose acetate matrix through Vander Waals interactions. In addition, the nitrogen atoms of the urethane bond formed between the free –OH groups on the surface of nanocellulose particles and isocyanates groups are also able to form hydrogen bonding with free and accessible ⎯OH groups on cellulose acetate. It is observed that increase in nanoparticle loading led to a corresponding increase in elongation at break. This trend was observed in all nanocomposite films prepared, similar to the literature reports (Benyoussif et al., 2015). This increase was within the range of strain values obtained for the controlled cellulose acetate film and the commercial cellulose acetate membrane. This implied that the addition of nanoparticles had little and /or no effects in some composite films. Toughness of the films was evidenced by their tensile energy absorption and the moduli of the nanocomposite films before fracturing. This property increased with increasing nanoparticle loading with exception of the control cellulose acetate film which had the lowest tensile index. In addition, the toughness of the films may be due to new interactions at the interface between nanoparticles, cellulose acetate and the plasticizers due to Vander Waal`s forces and hydrogen bonding (Pang et al., 2013). The stacking arrangement observed in the internal structure of the nanocomposite films as revealed by SEM images also provides evidence for the modulus and TEA values obtained and as well supports the toughness of the nanocomposite films. This property is essential for packaging applications. Low tensile strength and elongation at break point observed was linked to porosity of the nanocomposite films.

Trending in the nanocomposite films was also observed for their strain properties as the values were within the range obtained for the commercial cellulose acetate membrane and the control cellulose acetate film. This property was less affected by the nanoparticle content in films. This has been linked to the nanoparticle type synthesized. Due to their low elasticity, the films can be used as oil-adsorbents for up-take of oil film into their highly cellular and porous structure as revealed by SEM micrographs (**Plate 1**). In order to remove the oil after adsorption, the film could be treated by washing with suitable organic solvents (n-hexane or benzene) for clean-up and re-usability.

Screening of lactic acid bacteria for bacteriocin (bio-preservative) production

The nanocomposite films prepared were light/dense yellow films in terms of physical appearance. These nanocomposite films were used to filter microbial culture prepared at pH 3-5 and temperature 25-27 ^{o}C. Microbial agents employed for the production of biomolecules were *Bacillus, Enterococcus and Micrococcus species*. These filters were found efficient for the removal of the cell producing microorganisms from the biosynthesized molecules. Filtration gave rise to biomolecules solution which was free of the microbial species used for the synthesis of bacteriocin. The nanocomposite films were found efficient for the removal of microbial cells and were re-usable after sterilization in autoclave at 102 ^{o}C. The films had recoverability (450 nm) equivalence of 95.9 % based on R^2 = 0.959 of biomolecules (bacteriocin) produced.

Sensitivity Test of Clinical Bacterial Isolates against Acetate Reinforced Nanocomposite Films

The synthesized cellulose acetate reinforced nanocomposites films were tested against pure clinical bacterial isolates including *Pseudomonas aeruginosa* 1 and 2, *Proteus* sp, *Escherichia coli* and *Staphylococcus aureus* in order to evaluate the antibacterial properties of the films. **Table 4** shows the antibacterial activity of cellulose acetate nanocomposite films reinforced with different types of nanoparticle content against clinical isolates. It was observed that *Escherichia coli* and *Staphylococcus aureus* were not sensitive to the different nanocomposite films. *Pseudomonas aeruginosa* 1 and *Pseudomonas aeruginosa* 2 and *Proteus* had zones of clearance ranging from 1.8 to 2.5 mm.

Cellulose acetate nanocomposite film coded as A11/5% was prepared using H_3PO_4-propylcellulose nanoparticles. This film showed no antibacterial activity against all the tested bacteria. *Staphylococcus aureus* showed no zone of inhibition to all the cellulose acetate reinforced nanocomposite films with different loading. However, cellulose acetate reinforced nanocomposite film obtained using EDTA-modified cellulose nanoparticles as reinforcement with 20 % loading contents coded as (A2-EDTA/20) exhibited bacterial activity against *Pseudomonas* 2 and *Proteus* with inhibitory zones of 8 and 7 mm respectively. The highest activity of cellulose acetate nanocomposite film was recorded with H_3PO_4-cellulose acetate nanoparticles with loading content of 30 % A10(30) against *Pseudomonas* 1. The antimicrobial activities of cellulose acetate films impregnated with solution of bacteriophages against *salmonella typhimurium* (Delaine et al., 2015). Studies have shown that antibacterial properties of cellulose acetate films depend on the type of materials used for reinforcement, surface functionalities and/or chemical species with antibacterial properties (Perera et al., 2014). This study shows that cellulose acetate reinforced nanocomposite films with EDTA-modified H_3PO_4-cellulose nanoparticles, H_3PO_4-cellulose nanoparticles and H_3PO_4-cellulose acetate nanoparticles at various loading contents; EDTA H_3PO_4-CNPs (A2-EDTA/20 %), H_3PO_4-CNPs (A2/10 %), H_3PO_4-CANPs (A10/30 %) and (A10/40 %) showed antibacterial properties. The antibacterial properties of films have been attributed to the ability of the negatively charged phosphate groups, oxygen atoms, carbonyl group, nitrogen

atoms with lone pairs, and their ability to interact with the organisms, thereby inhibiting their growth and activities. The presence of these groups was revealed by FT-IR results of the H_3PO_4-modified nanoparticles and nanocomposite films (Youssef et al., 2006; Pacheco et al., 2012; Granja et al., 2001; Azeh et al., 2017). The antibacterial properties of the cellulose acetate reinforced nanocomposite films could help prevent biofouling when used as water filter. The results of sensitivity test of the films showed that the prepared films could find useful applications in packaging and preservation. Pure cellulose acetate film used as control did not show antibacterial properties against the tested organisms, probably due to lack of such groups on its surface. Increase in loading contents of the various types of nanoparticles may improve the antibacterial properties of the nanocomposite films.

Table 2: Weight percent gain (WPG) in modification using Anhydrous EDTA

S/N	Sample	Time (h)	WPG (%)
1	A2	2.0	53.8
2	A11	2.0	50.8
3	Native-cellulose	2.0	56.5

Table 3: Weight Percent Gains (WPGs) in Modification Using TDI

S/N	Sample	Time (h)	WPGs (%)
1	A2	24.0	59.5
2	A11	24.0	57.4
3	Native Cellulose	24.0	64.8

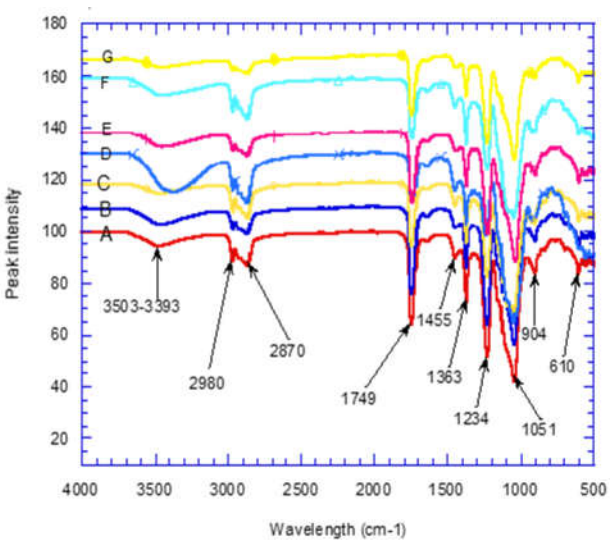

Figure 1: FT-IR Spectra of (A) CNCs-20; (B) CNCs-30; (C) CNCs-40; (D) CNCs-10; (E) CNC-EDTA-10; (F) MC-5; (G) NPC-50

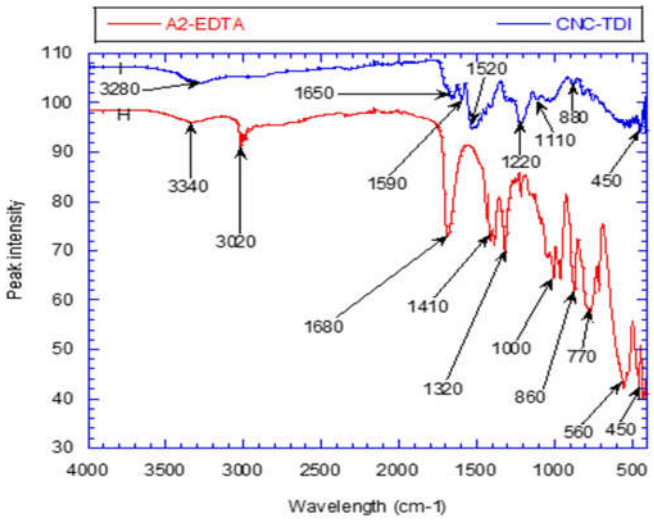

Figure 2: FT-IR of modified cellulose nanocrystals CNC-EDTA (H) and CNC-TDI (I)

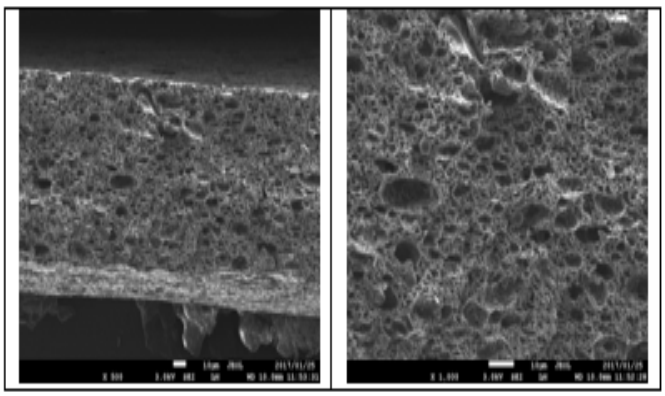

Plate 1: SEM micrographs of nanocomposite films

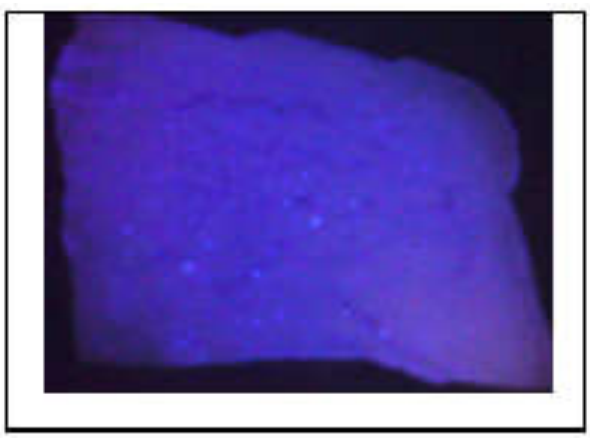

Plate 2: Fluorescence photo image of cellulose acetate reinforced nanocomposite film

 This journal is © The Nigerian Young Academy 2020

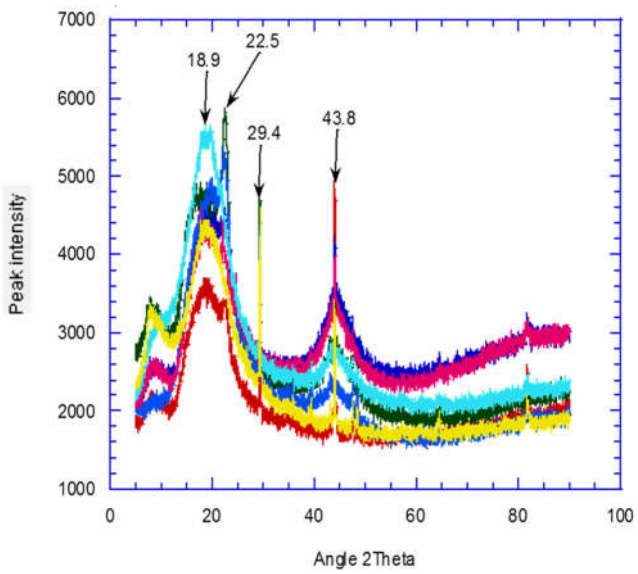

Figure 3: XRD of nanocomposite films with different nanoparticle compositions
A2-20; A2-30; A2-40; A2-10; A2-N2/20; MC/5 and PC/50 wt %

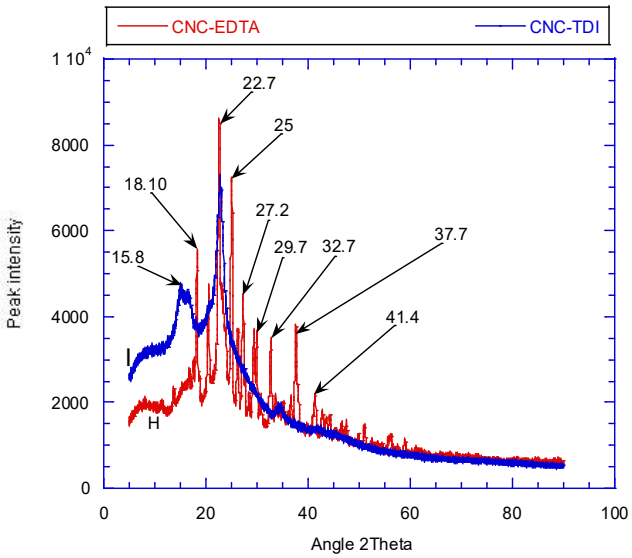

Figure 4: XRD Diffractograms for CNC-EDTA (H) and CNC-TDI (I)

Table 4: Zone of Clearance of Clinical Isolates Collected from UITH by Cellulose Acetate Reinforced Nanocomposite Films

S/N	Clinical Isolates	Zones of clearance (mm)					Control
		A2/10	A10/30	A10/40	A2-EDTA/20	A11/5	(Pure CA Film)
1	*Pseudomonas aeruginosa* 1	0.0	2.5	2.5	0.0	0.0	0.0
2	*Pseudomonas aeruginosa* 2	2.3	0.0	0.0	2.0	0.0	0.0
3	*Proteus* sp	0.0	0.0	0.0	1.8	0.0	0.0
4	*Escherichia coli*	0.0	0.0	0.0	0.0	0.0	0.0
5	*Staphylococcus aureus*	0.0	0.0	0.0	0.0	0.0	0.0

Conclusion

Room temperature cellulose acetate nanocomposite thin films were prepared by solution casting. Effects of modification and filler loading on films were revealed by FT-IR, SEM, Tensile and XRD results. The nanocomposite films were useful in removing the microorganisms from crude bacteriocin solution of the biosynthesized molecules. These films also showed blue fluorescence at long wavelength under the UV-lamp at 360 nm and may find applications as good and fast analytical tools such as a biosensor. The synthesized films showed antibacterial properties against clinical isolates of *Pseudomonas* 1, 2 and *Proteus* sp.

Conflict of Interests

All Authors have declared that there are no conflicts of interest.

Authors' Contributions

Conception: FAA, GAO, YA, DOA
Design: YA, DOA, FAA, GAO
Execution: YA, DOA, FAA, GAO
Interpretation: YA, DOA, FAA
Writing the paper: DOA, YA, FAA

References

Andrea, G. P. R. F., Ana, R. P. F., Ana, A. V., Susana, C. M. F., Teodoro, P., Eva, R. A., Ana, B. T., Armando, J. D. S., Carlos, P. N., Carmen, S. R. F., 2013, Biocompatible bacterial cellulose-poly (2-hydroxyethyl methacrylate) nanocomposite films. BioMed Research International, 1-14.

Azeh, Y., Olatunji, G. A., Adekola, F. A., 2017, Synthesis and characterization of cellulose nanoparticles and its derivatives using a combination of spectro-analytical techniques. International Journal of Nanomedicine & Engineering. **2**(6): 65-94.

Bauer A. W., Kirby, W. M. M., Sherries, S. C., Turk, M., 1966, Antibiotic susceptibility testing by a standard single disc method. American Journal of Clinical Pathology, **36**:492-496.

Benyoussif, Y., Aboulhrouz, S., El-Achaby, M., Cherkaoui, O., Lallam, A., El-Bouchti, M., Zahouily, M., 2015, Preparation and properties of

bionanocomposite films reinforced with nanocellulose isolated from Moroccan alfa fibres. Autex Research Journal, **15**(3): 64-72.

Delaine, M. G., Gegina, C. S. M., Maryoris, L. S., Renato, S. C., 2015, Acetate film with bacteriophages for potential antimicrobial use in food packaging, LWT-Food Science and Technology, **63**: 85-91.

Ekwem, O. H., 2014, Isolation of antimicrobial producing actobacilli from *akamu* (A Nigerian fermented cereal gruel). African Journal of microbiology Research, **8**(7): 718-720.

Fernando, G. T., Solene, C., Omar, P. T., 2012, Biocompatibility of bacterial cellulose based biomaterials. Journal of Functional Biomaterials, **3**(4): 864-878.

Fogorasi, M. S., Barbu, I., 2017, The potential of natural fibres for automotive sector – review. IOP Conf. Ser.: Materials Science Engineering, **252**: 1-10.

Giorgi, M., Linus, W., Eva, E., Sandor, B., Maria, S., Albert, M., 2014, A size-exclusion nanocellulose filter paper for virus removal. Advanced Healthcare Materials, **3**: 1546–1550.

Golkar, Z., Bagazra, O., Pace, D. G., 2014, Bacteriophage therapy: a potential solution for the antibiotic resistance crisis. Journal of Infection in Developing Countries, **8**(2):129–136.

Granja, P. L., Pouysegu, L., Pe,′Traud, M., De JeSo, B., Baquey, C., Barbosa, M. A., 2001, Cellulose Phosphates as Biomaterials. I. Synthesis and characterization of highly phosphorylated cellulose gels. Journal of Applied Polymer Science, **82**: 3341–3353.

Huang, B., Tang, L., Dai, D., Ou, W., Li, T., Chen, X., 2011, Preparation of nanocellulose with cation–exchange resin catalysed hydrolysis, Biomaterials Science and Engineering, Rosario Pignatello (Ed.). London, UK.

Jinhui, P., Xin, L., Xueming, Z., Yuying, W., Runcang, S., 2013, Fabrication of cellulose film with enhanced mechanical properties in ionic liquid 1-allyl-3-methylimidaxolium chloride (AmimCl). Materials, **6**: 1270-1284.

Kalia, S., Kaith, B. S., Kaur, I., 2011, Cellulose Fibers: Bio- and Nano-Polymer Composites. Green Chemistry and Technology. Springer-Verlag Berlin Heidelberg, Switzerland.

Kusworo, T. D. B., Wibowo, A. I., Harjanto, G. D., Yudisthira, A. D., Iswanto, F. B., 2014, Cellulose acetate membrane with improved perm-selectivity through modification dope composition and solvent evaporation for water softening. Research Journal of Applied Sciences, Engineering and Technology, **7**(18): 3852-3859.

Lacroix, M., Khan, R. A., Salmieri, S., Huq, T., Khan, A., Safrany, A., 2011, Production and Properties of Nano Fiber (NCC) and Nano Tube (CNT) Reinforced Biodegradable Packaging Films: Effect of Gamma Radiation (IAEA-RC--12071). International Atomic Energy Agency (IAEA).

Lexa, G., 2014, Morphological, mechanical and rheological behaviour of cellulose nanocrystal poly (methyl methacrylate) nanocomposites prepared by wet ball milling and melt mixing. M.Sc. Thesis Submitted to the School of Graduate Studies McMaster University.

Marianne, L. T., Claire, P., Thierry, C., Jean-Pierre, B., Agnes, S., 2007, Physico-chemical modifications of the interactions between hemp fibres and a lime mineral matrix: impacts on mechanical properties of mortars, 10th International Conference of the European Ceramic Society, Berlin, Germany.

Marielle, H., Lars, A. B., 2007, Structure and properties of cellulose nanocomposite films containing melamine formaldehyde. Journal of Applied Polymer Science. **106**: 2817–2824.

Meiling, Y., Shujun, L., Mingxin, Z., Chunjie, L., Feng, D., Wei, L., 2013, Characterization of surface acetylated nanocrystalline cellulose by single-step method. BioResources, **8**(4): 6330-6341.

Nadezhda, R., Lachezar, R., Sanchi, N., Isabel, M. M. S., Maria, H. V. F., Michael, H., 2011, Methylcellulose/Sio_2 Hybrids: Sol-Gel Preparation and Characterization by XRD, FTIR and AFM. Central European Journal Chemistry. **9**(1): 112-118.

Nor, F., Mat, Z., Salma, M. Y., Ishak, A., 2014, Preparation and characterization of cellulose and nanocellulose from pomelo (Citrus grandis) Albedo. Journal of Nutrition and Food Sciences, **5**(1) :1-4.

Pacheco, D. M., Johnson, J. R., and Koros, W. J., 2012, Aminosilane-functionalized cellulosic polymers for increased carbon dioxide sorption. Industrial & Engineering Chemistry Research, **51**(1):503-514.

Pang, J., Liu, X., Zhang, X., Wu, Y., Sun, R., 2013, Fabrication of cellulose film with enhanced mechanical properties in ionic liquid 1-Allyl-3-methylimidaxolium chloride (AmimCl). Materials, **6**(4): 1270-1284.

Perera, D. H. N., Nataraj, S.K., Thomson, N. M., Sepe, A., Huttner, S., Steiner, U., Qiblawey, H., Sivaniah, E., 2014, Room-temperature development of thin film composite reverse osmosis membrane from cellulose acetate with antibacterial properties. Journal of Membrane Science, **453**: 212-220.

Renata, P. H. B., Maria, V. G., Fabio, Y., 2012, Films of starch and poly (butylene adipate co-terephthalate) added of soybean oil (SO) and Tween 80. Carbohydrate Polymers. **90**: 1452 – 1460.

Samuel, E., Wim, T., 2014, Surface modification of cellulose nanocrystals. The Royal Society of Chemistry, Nanoscale. **6**: 7764-7779.

Samzadeh, K. A., Esfandiary, N., 2016, Synthesis and characterization of new biodegradable chitosan/polyvinyl alcohol/cellulose nanocomposite. Advances in Nanoparticles, **5**: 18-26.

Sani, S. D. M., Deme, J. J. I., 2013, Isolation and screening of lactic acid bacteria from fermented milk products for bacteriocin production. Annals. Food Science and Technology, **14**(1): 122-128.

Saxena, A. 2013, Nanocomposites based on nanocellulose whiskers. Published dissertation presented to the academic faculty in partial fulfillment of the requirements for the degree Doctor of philosophy in the school of Chemistry and Biochemistry, Georgia Institute of Technology.

Simone, M. L. R., Noor, R., Maria, I. G. D. M., Sonia, M. B. N., Clara, I. D. B., 2012, Chlorine-free extraction of cellulose from rice husk and whisker isolation. Carbohydrate Polymers, **87**: 1131 – 1138.

 This journal is © The Nigerian Young Academy 2020

Syuhada, N. I., Huang, N. M., Vijay, S. K., Lim, H. N., Rahman, S. A., Thien, G. S. H., Ibrahim, N. A., Ahmad, M., Moradihamedani, P., 2014, Enhanced Mechanical Properties of Chitosan/ EDTA-GO Nanocomposites Thin Films (Peningkatan Sifat Mekanik Filem Nipis Nanokomposit Kitosan/EDTA- GO). Sains Malaysiana, **43(6)**: 851–859.

Tanzina, H., Stephane, S., Avik, K., Ruhul, A., Khan, C. L. T., Bernard, R., Carole, F., Jean, B., Jorge, U. C., Musa, R. K., Monique, L., 2012, Nanocrystalline cellulose (NCC) reinforced alginate based biodegradable nanocomposite film. Carbohydrate Polymers. **90**: 1757– 1763.

Wan, Y. Z., Honglin, L., He, F., Liang, H., Li, X. L., 2019, Mechanical, moisture absorption, and biodegradation behaviours of bacterial cellulose fibre-reinforced starch biocomposites. Composites Science and Technology, **69**: 1212–1217.

Wienk, I. M., Boom, R. M., Beerlage, M. A. M., Buulte, A. M. W., Smolders, C. A., Strathmann, H., 1996, Recent advances in the formation of phase inversion membranes made from amorphous or semi-crystalline polymer. Journal of Membrane Science, **113**(2): 361-371.

Wright, G. D., 2014, Something new: Revisiting natural products in antibiotic drug discovery. Canadian Journal of Microbiology, **60**(3):147–154.

Yiying, Y. B. S., 2007, A comparative study of cellulose I and II fibers and nanocrystals. M.Sc. Thesis Submitted to the Graduate Faculty of the Louisiana State University and Agricultural and Mechanical College, School of Renewable Natural Resources, Heilongjiang Institute of Science and Technology.

Yoshifumi, A., Toyotoshi, U., 2013, Solid-phase extraction of Pb from common salt and water samples by cellulose modified with anhydrous EDTA. Cellulose Chemistry and Technology, **47**(5-6): 479-486.

Youssef, H., Henri, C., Michel, R. V., 2006, TEMPO-mediated surface oxidation of cellulose whiskers. Cellulose, **13**: 679 –687.

Yucheng, P., Douglas, J. G., Yousoo., H., Alper, K., Zhiyong, C., Mandla, A. T., 2013, Influence of drying method on the material properties of nanocellulose I: Thermostability and crystallinity. Cellulose, **20**: 2379–2392.

Zhao, Y., Sugiyama, S., Miller, T., Miao, X., 2008, Nanoceramics for blood-borne virus removal. Expert Review of Medical Devices, **5**(3): 395 - 405.